Report

Cell Reports

TALEN Gene Knockouts Reveal No Requirement for the Conserved Human Shelterin Protein Rap1 in Telomere Protection and Length Regulation

Graphical Abstract

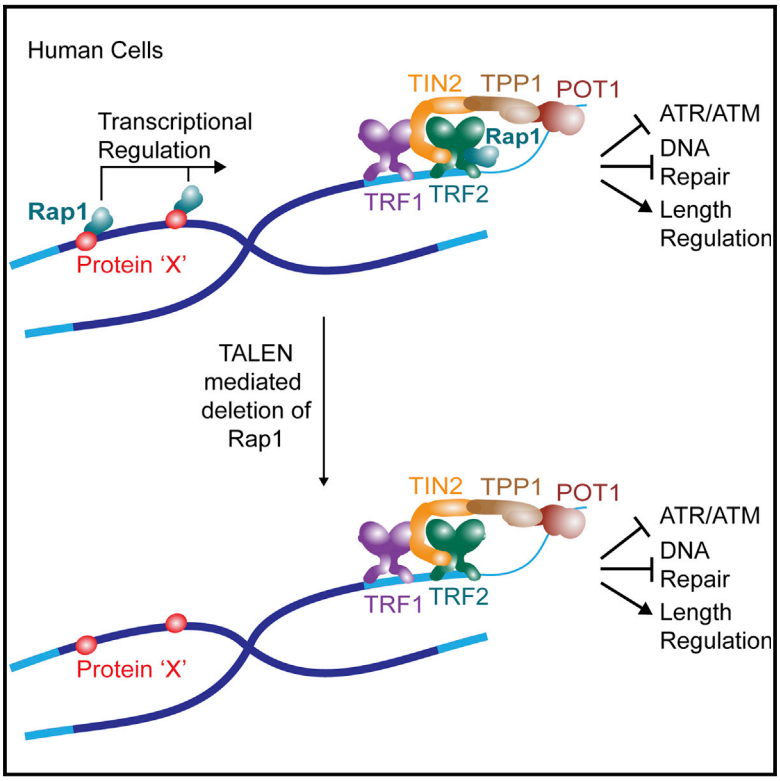

Highlights

TALENs were used to delete the gene for the conserved Rap1 subunit of shelterin

Rap1 targeting was efficient in several immortalized human cell lines

Rap1 knockout did not induce telomere fusions, length changes, or other telomere defects

Rap1 conservation may reflect its transcriptional rather than telomeric function

Authors

Shaheen Kabir, Dirk Hockemeyer, Titia de Lange

Correspondence

delange@mail.rockefeller.edu

In Brief

Kabir et al. now employ a TALEN-mediated genome editing strategy to make Rap1 knockouts in a diverse array of human cell lines and test the function of this conserved telomere protein. They find that, unlike its yeast counterparts, mammalian Rap1 is not essential for telomere protection or length regulation, but its role in transcriptional regulation is maintained, indicating why Rap1 remains so conserved.

Accession Numbers

GSE61900

Kabir et al., 2014, Cell Reports 9, 1273–1280
November 20, 2014 ©2014 The Authors
http://dx.doi.org/10.1016/j.celrep.2014.10.014

Cell Reports
Report

TALEN Gene Knockouts Reveal No Requirement for the Conserved Human Shelterin Protein Rap1 in Telomere Protection and Length Regulation

Shaheen Kabir,[1] Dirk Hockemeyer,[2] and Titia de Lange[1,*]
[1]Laboratory for Cell Biology and Genetics, The Rockefeller University, New York, NY 10065, USA
[2]Department of Molecular and Cellular Biology, University of California, Berkeley, Berkeley, CA 94720, USA
*Correspondence: delange@mail.rockefeller.edu
http://dx.doi.org/10.1016/j.celrep.2014.10.014

SUMMARY

The conserved protein Rap1 functions at telomeres in fungi, protozoa, and vertebrates. Like yeast Rap1, human Rap1 has been implicated in telomere length regulation and repression of nonhomologous end-joining (NHEJ) at telomeres. However, mouse telomeres lacking Rap1 do not succumb to NHEJ. To determine the functions of human Rap1, we generated several transcription activator-like effector nuclease (TALEN)-mediated human cell lines lacking Rap1. Loss of Rap1 did not affect the other components of shelterin, the modification of telomeric histones, the subnuclear position of telomeres, or the 3′ telomeric overhang. Telomeres lacking Rap1 did not show a DNA damage response, NHEJ, or consistent changes in their length, indicating that Rap1 does not have an important function in protection or length regulation of human telomeres. As human Rap1, like its mouse and unicellular orthologs, affects gene expression, we propose that the conservation of Rap1 reflects its role in transcriptional regulation rather than a function at telomeres.

INTRODUCTION

Rap1 is a component of shelterin, the protein complex that functions to protect telomeres, recruits telomerase, and regulates telomere length (reviewed in Palm and de Lange, 2008). Human shelterin contains two double-stranded (ds) telomeric DNA binding proteins, TRF1 and TRF2, which both interact with TIN2. TIN2 in turn binds heterodimers of TPP1 and the POT1 single-stranded (ss) telomeric DNA binding factor. Mammalian Rap1 relies on TRF2 to localize to telomeres (Li et al., 2000). Similarly, the Rap1 orthologs of fission yeast and trypanosomes use a TRF1/2-like protein to accumulate at telomeres (Kanoh and Ishikawa, 2001; Yang et al., 2009). In contrast, budding yeast Rap1 binds telomeric DNA directly (Konig et al., 1996).

Rap1 was discovered as a *Saccharomyces cerevisiae* transcriptional regulator (repressor/activator protein) (Shore and Nasmyth, 1987). All Rap1 proteins have an N-terminal BRCT motif, a C-terminal protein interaction domain, and one or two central Myb domains (Konig et al., 1996; Liu and Lustig, 1996; Hardy et al., 1992a; Wotton and Shore, 1997; Yang et al., 2009; Kanoh and Ishikawa, 2001; Li et al., 2000). Budding yeast Rap1 binds to promoter and silencer elements and interacts with the silencing proteins Sir3p and Sir4p (Hardy et al., 1992a, 1992b; Shore, 1994; Lickwar et al., 2012; Cockell et al., 1995). Although mammalian Rap1 does not interact with sirtuins, it localizes to chromosome-internal sites and controls gene expression, affecting metabolism and body weight control (Yeung et al., 2013; Martínez et al., 2013; Yang et al., 2011). Rap1 also regulates gene transcription in fission yeast and in the distantly related trypanosomes (Kanoh and Ishikawa, 2001; Yang et al., 2009).

It is unclear which telomeric functions of Rap1 are conserved between yeast and mammals. Rap1 controls telomere length in yeast, acting to inhibit inappropriate telomere elongation (Lustig et al., 1990; Conrad et al., 1990; Sussel and Shore, 1991; Kyrion et al., 1992; Kanoh and Ishikawa, 2001). This control of telomere length is largely mediated by the Rap1-interacting factors Rif1 and Rif2 (Hardy et al., 1992a; Wotton and Shore, 1997; Levy and Blackburn, 2004; Teixeira et al., 2004). In support of a role in telomere length control, small hairpin RNAs (shRNAs) to human Rap1 induce telomere lengthening (O'Connor et al., 2004), as do overexpression of several Rap1 truncation mutants (Li and de Lange, 2003). However, Rap1 knockout mice show no change in telomere length, even after three generations (Sfeir et al., 2010). Additionally, mammalian Rif1 is not localized at telomeres (Silverman et al., 2004; Xu and Blackburn, 2004), and there is no mammalian ortholog of Rif2.

It is also unclear whether the role of Rap1 in protection of telomeres from nonhomologous end-joining (NHEJ), which has been demonstrated in yeast (Pardo and Marcand, 2005; Miller et al., 2005), is conserved in mammals. In vitro, human Rap1 can block NHEJ when it binds to TRF2 loaded on an end-joining substrate (Bae and Baumann, 2007), and a Rap1-fusion protein can reduce telomere fusions when it is tethered to telomeres that are depleted of TRF2 (Sarthy et al., 2009). On the other hand, mouse cells lacking Rap1 show no telomere fusions and Rap1-deficient mice are alive and fertile (Sfeir et al., 2010; Martinez et al., 2010). The only telomere deprotection phenotype in Rap1-deficient mouse cells is a propensity for telomere-telomere recombination when Ku70/80 are also absent (Sfeir et al., 2010).

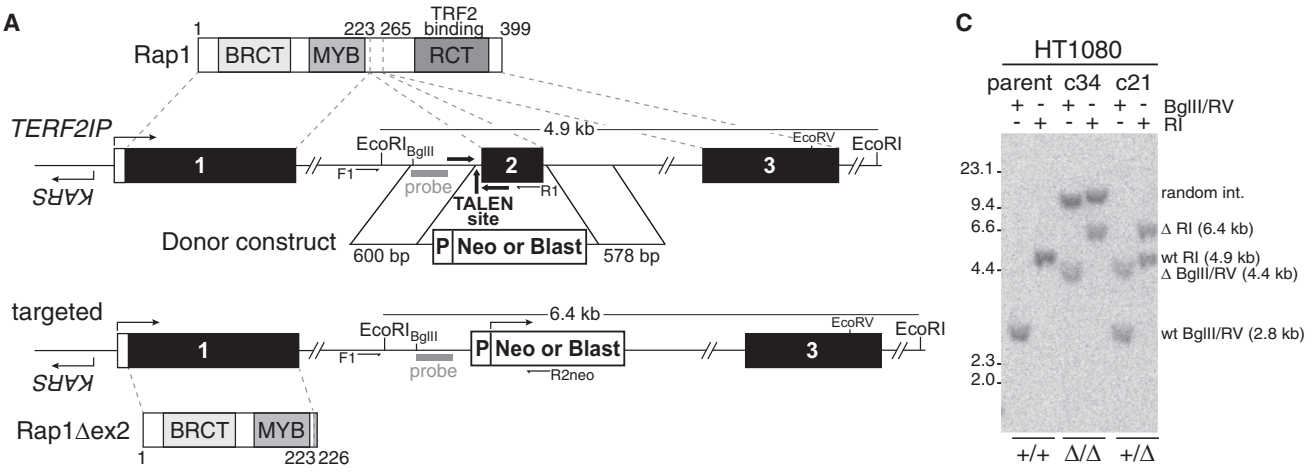

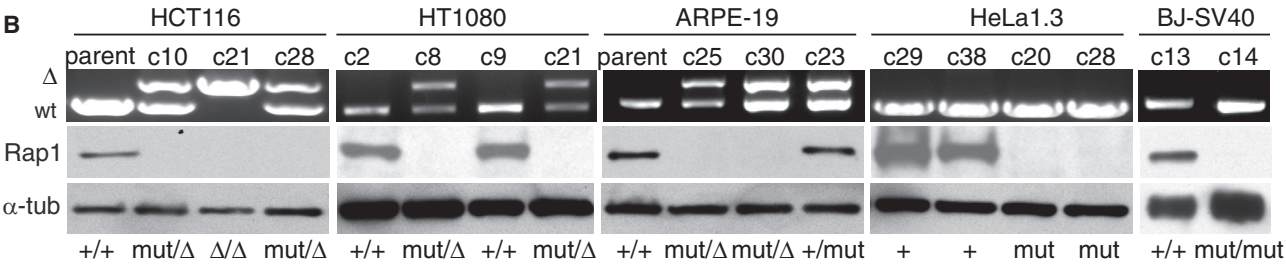

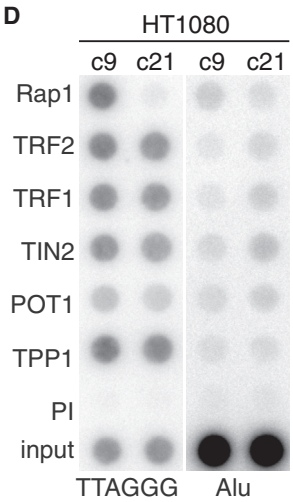

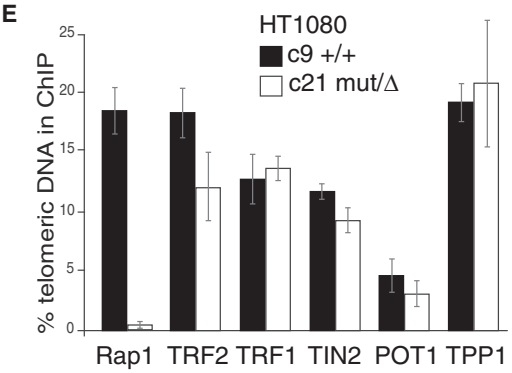

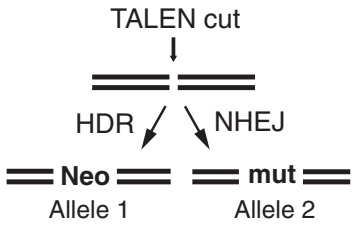

G

Cell line	Primary screening	Clones w/o Rap1 protein (% of total)	Clones w/ neo in both alleles	Clones w/ muts in one allele	Clones w/ muts only
HCT116	PCR (neo)	10 (65%)	3	7	n/a
HT1080	PCR (neo)	11 (36%)	1	10	n/a
ARPE-19	PCR (neo)	6 (24%)	0	6	n/a
HeLa1.3	Immunobl	8 (21%)	0[a]	0	8
BJ-SV40(neo)	Immunobl	1[b](3%)	0[a]	0	1

[a] no insertion of the blasticidin cassette into the Rap1 locus ;
[b] this clone succumbed in crisis

(legend on next page)

To determine the function(s) of human Rap1, we used transcription activator-like effector nucleases (TALENs) to knock out the *TERF2IP* gene. Analysis of several independent Rap1-deficient cell lines demonstrated that human Rap1 was not required for telomere protection, telomere length regulation, and other aspects of telomere function. In contrast, we document a change in the transcription of several genes upon loss of Rap1, suggesting that its transcriptional function is primarily responsible for the high degree of Rap1 conservation from unicellular organisms to mammals.

RESULTS

Efficient TALEN-Mediated Knockout of Human Rap1

The human Rap1-encoding *TERF2IP* gene shares its promoter region with the essential *KARS* (lysyl-tRNA synthetase) gene located just upstream of exon 1 (Figure 1A). To avoid disrupting the *KARS* gene, we employed TALENs to delete exon 2, a targeting strategy analogous to the one used for mouse *TERF2IP* (Sfeir et al., 2010) (Figures 1A, S1A, and S1B). Deletion of exon 2 should result in an mRNA encoding a 226 aa open reading frame (ORF) that ends prematurely in a stop codon at the beginning of exon 3. As exon 3 encodes the TRF2-binding domain, the truncated Rap1 protein is not expected to localize to telomeres. Taking advantage of the small size of exon 2 (125 bp) and anticipated resection of TALEN-induced double-strand breaks (DSBs) (Chen et al., 2011; Urnov et al., 2010), a neomycin donor construct was designed containing 5′ and 3′ arms homologous to the surrounding introns. Homology-directed repair (HDR) using the donor construct should result in deletion of exon 2 and insertion of the neomycin cassette.

TERF2IP was targeted in two near-diploid cancer lines (HCT116 colorectal carcinoma and HT1080 fibrosarcoma), a subclone of the near-triploid cervical carcinoma HeLa cell line (HeLa1.3; Takai et al., 2010), the diploid ARPE-19 retinal pigment epithelial cell line, and primary BJ fibroblasts transformed with SV40 large T antigen (SV40LT). With the exception of SV40LT BJ, all cells expressed telomerase. For HCT116, HT1080, and ARPE-19 cells, neomycin resistant clones were obtained, analyzed by PCR, and then evaluated by Southern blotting to verify the correct neomycin insertion (Figures 1B and 1C). For HeLa1.3 and BJ, the blasticidin donor construct was used and clones were analyzed by immunoblotting for Rap1. This analysis identified clones that lacked the wild-type *TERF2IP* gene and expressed no detectable Rap1 protein (Figures 1B, 1C, and S1C). We were unable to detect the polypeptides representing the remaining ORF of the targeted *TERF2IP* gene (Figures S1D–S1F), perhaps due to nonsense-mediated decay.

Unexpectedly, immunoblotting revealed the complete loss of Rap1 in heterozygous clones with one neo insertion (Figures 1B and S1C). Telomeric chromatin immunoprecipitation (ChIP) of two such clones (HT1080 c21 and HeLa1.3 c28) confirmed that Rap1 was absent from telomeres (Figures 1D, 1E, S1G, and S1H). Sequencing revealed small deletions close to the TALEN site in these and other Rap1-deficient clones with only one neo-containing *TERF2IP* gene (Figure S1B). Most mutations had ablated Rap1 by deleting the exon 2 splice acceptor site or had created a frameshift mutation, indicating that errors generated during NHEJ had inactivated the *TERF2IP* gene (Figure 1F). As a result, the frequency of the *TERF2IP* knockouts (KOs) is much higher than deduced from PCR genotyping. Taking the deleterious repair events into account, the ablation of Rap1 occurred at 20%–65% efficiency in HCT116, HT1080, and ARPE-19 cells (Figure 1G). The HCT116 cells showed the highest KO frequency consistent with their propensity for HDR (reviewed in Sedivy et al., 1999). The actual KO frequency is probably even higher, as only clones with a neo cassette in the *TERF2IP* gene were analyzed.

The high KO frequency allowed screening of HeLa1.3 and SV40LT BJ clones by Rap1 immunoblotting. Sequencing of Rap1-negative HeLa1.3 clones revealed that all three alleles in this cell line contained inactivating mutations near the TALEN cut site (Figure S1B). Prolonged culturing of clones in blasticidin resulted in cell death, suggesting that the EF-1 alpha promoter (pEF) blasticidin cassette did not confer long-term resistance. The KO frequency was lower in SV40LT BJ fibroblasts with only one blasticidin-resistant clone showing absence of Rap1 protein. This clone was not analyzed because it perished in telomere crisis, as did many of the Rap1-proficient SV40LT BJ clones.

Rap1-Deficient Cells Proliferate and Maintain Fully Protected Telomeres

The Rap1-deficient cell lines proliferated normally (Figure 2A) and lacked a significant level of telomere dysfunction-induced foci (TIFs), a readout for telomere damage (Figures 2B and 2C), indicating that removal of Rap1 from telomeres does not result in a DNA damage response.

Cells lacking Rap1 also did not show a significant induction of DSB repair at telomeres (Figures 2D and 2E). Metaphase spreads of Rap1 KOs lacked chromosome end fusions, a readout for telomeric NHEJ. Chromosome orientation (CO) fluorescence in situ hybridization (FISH) to monitor HDR-mediated telomere-sister chromatid exchanges (T-SCEs) established

Figure 1. TALEN-Mediated Inactivation of the Gene for Human Rap1

(A) Schematic of human Rap1, the *TERF2IP* locus, the targeting construct, and the resulting knockout allele. F1, R1, and R2neo: PCR primers for genotyping. Arrows in bold: TALEN binding and cut sites.

(B) PCR genotyping of the *TERF2IP* gene and western blotting for Rap1 in the indicated clones. +, WT allele; Δ, targeted allele; mut, mutation resulting in loss of Rap1.

(C) Southern blot of EcoRI (RI)- or BglII/EcoRV (RV)-digested genomic DNA from targeted HT1080 clones. Probe shown in (A).

(D) Telomeric ChIP of WT and targeted HT1080 clones. Duplicate dot-blots were probed for telomeric or Alu repeats.

(E) Average percentage of telomeric DNA recovered in ChIPs with the indicated antibodies (two independent experiments). Error bars represent SEM.

(F) Schematic illustrating NHEJ and HDR after TALEN cutting.

(G) Table indicating number of Rap1 knockout clones acquired and the genetic alterations in *TERF2IP*.

See also Figure S1.

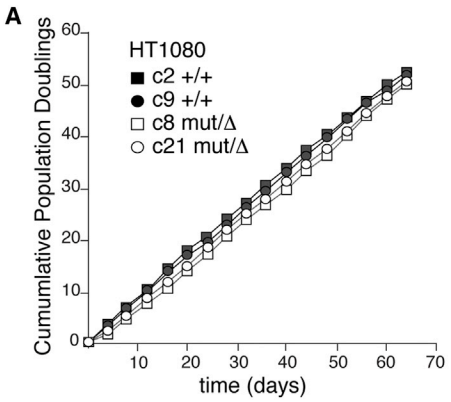

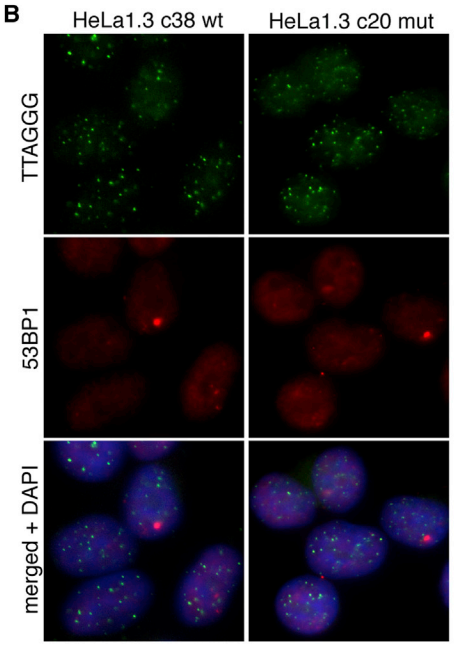

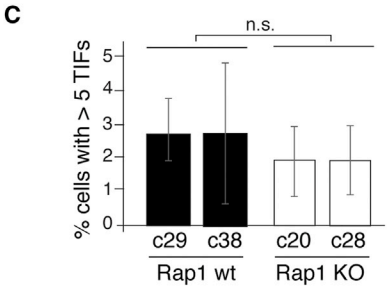

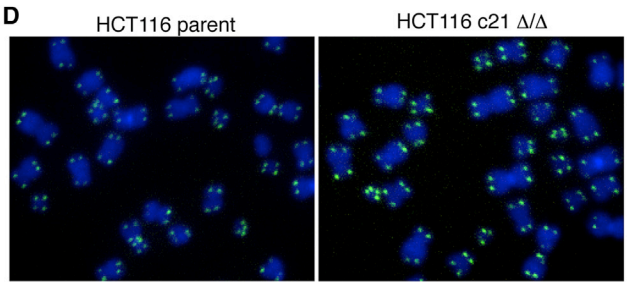

E

Cell line	Rap1 status	number of telomeres scored	% of telomeres fused (av±SD)	
HeLa1.3 c29	+/+/+	1084, 932, 1008	0.27±0.2	p=0.084
HeLa1.3 c38	+/+/+	1002, 1110, 1004	0.40±0.4	
HeLa1.3 c20	mut/mut/mut	1028, 1002, 1060	0.85±0.5	
HeLa1.3 c28	mut/mut/mut	1010, 992, 1044	0.92±1.0	
HCT116 parent	+/+	952, 920	0.21	
HCT116 c8	mut/Δ	1100, 600	0.18	
HCT116 c21	Δ/Δ	1068, 852	0.23	
ARPE-19 c23	+/+	956	<0.1	
ARPE-19 c25	mut/Δ	1008, 800	0.2	
HT1080 c9	+/+	1020	0.39	
HT1080 c21	mut/Δ	1120	0.36	

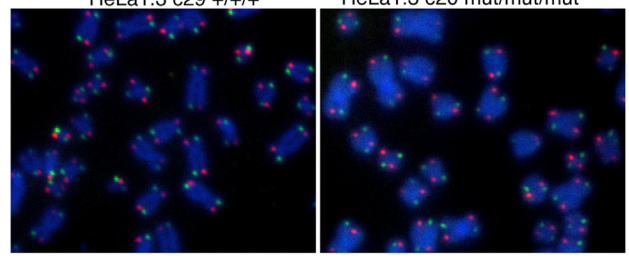

G

Cell line	Rap1 status	number of telomeres scored	%T-SCE	
HeLa1.3 parent	+/+/+	1232	3.3	p=0.8
HeLa1.3 c29	+/+/+	1876	3.3	
HeLa1.3 c38	+/+/+	2112	3.0	
HeLa1.3 c20	mut/mut/mut	1298	4.3	
HeLa1.3 c27	mut/mut/mut	1074	1.9	
HeLa1.3 c28	mut/mut/mut	1746	4.5	
HeLa1.3 c35	mut/mut/mut	2148	3.0	

Figure 2. Telomere Protection in Rap1-Deficient Cells

(A) Growth curves of WT and Rap1 KO HT1080 clones.

(B) TIF assay on WT and KO HeLa1.3 clones. Green, telomeric FISH; red, immunofluorescence for 53BP1; blue, DNA (DAPI).

(C) Quantification of TIF assay (see B). Error bars represent SDs of three independent experiments (n ≥ 100 nuclei per clone). p values from a two-tailed paired t test combining WT and KO data sets. n.s., not significant.

(D) Metaphase chromosomes from the indicated WT and Rap1 KO cells. Green, telomeric FISH; blue, DNA (DAPI).

(E) Quantification of telomere fusions, detected as in (D), in the indicated clones. p values from a two-tailed paired t test on combined WT and KO data sets.

(F) CO-FISH analysis on the indicated WT and KO HeLa clones.

(G) Table showing the percentage of telomeres showing T-SCEs as assayed in (F) in the indicated clones. p value from unpaired two-tailed t test.

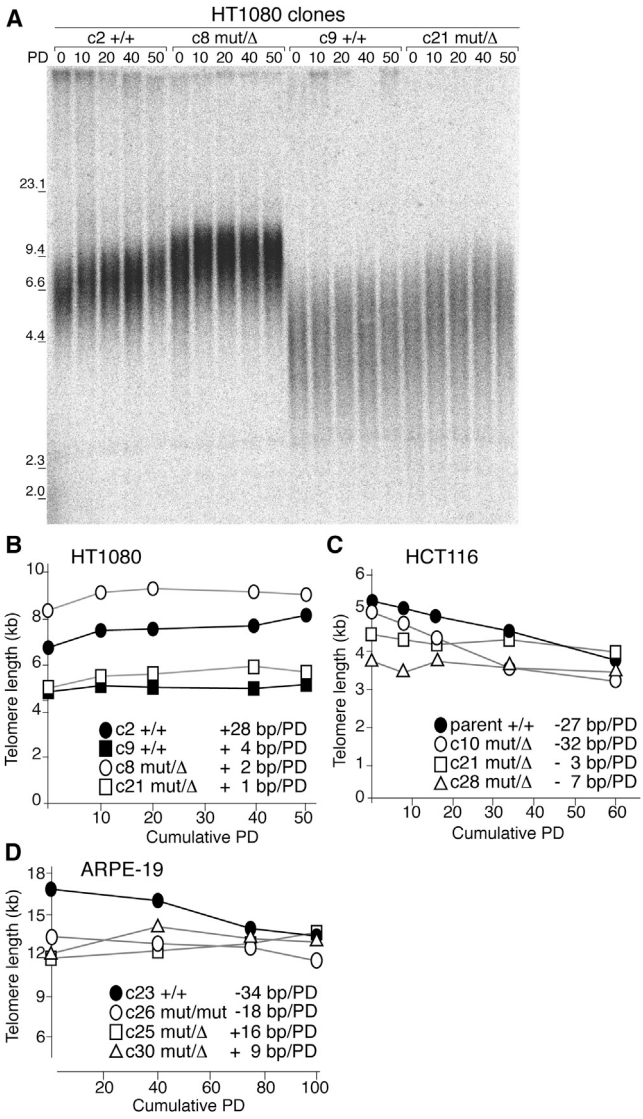

Figure 3. Loss of Rap1 Does Not Affect Telomere Structure

(A) Southern blot of telomeric restriction fragments from two WT and two KO HT1080 clones at the indicated PDs.

(B–D) Curves of average telomere lengths at indicated PDs in HT1080, HCT116, and ARPE-19 clones, respectively.

See also Figure S2.

that recombination remained repressed at telomeres (Figures 2F and 2G). Thus, human telomeres remain protected from NHEJ and HDR in the absence of Rap1.

Unaltered Telomere Length Dynamics in the Absence of Rap1

To determine whether Rap1 affected telomere length homeostasis, two HT1080 Rap1-deficient clones were cultured for 50 population doublings (PD) alongside two Rap1-proficient clones selected for their matching telomere lengths (Figure 3A). All clones exhibited a mild increase in telomere length (Figure 3B). The two Rap1-deficient clones lengthened their telomeres at a similar modest rate (1–2 bp/PD), whereas the two Rap1-proficient clones differed in the rate of telomere lengthening (28 and 4 bp/PD) (Figure 3B). Given the clonal variation and small differences in telomere length changes, the removal of Rap1 did not appear to have a strong effect on telomere length dynamics in HT1080 cells.

Similarly, Rap1 did not affect the telomere length dynamics of HCT116 clones (Figure 3C). Two Rap1-deficient clones showed telomere shortening at variable rates (−3 to −32 bp/PD). Given that the telomere shortening in the parental cells (−27 bp/PD) is similar to that of one of the Rap1-deficient clones (c10), we conclude that also in HCT116 cells, Rap1 did not strongly affect telomere dynamics.

Finally, three Rap1-deficient ARPE-19 clones (c26, c25, and c30) showed wide variations in telomere dynamics, ranging from slight shortening (−18 bp/PD) to slight elongation (9 and 16 bp/PD) (Figure 3D). The single Rap1-proficient clone (c23) showed telomere shortening at a rate of −34 bp/PD. Thus, there is considerable variability in the telomere dynamics in ARPE-19 clones but no consistent effect of Rap1 deletion.

Given the lack of consistent shortening or lengthening phenotypes in multiple Rap1 KOs, the simplest interpretation is that Rap1 does not play a major role in telomere length regulation. Deletion of Rap1 also did not induce an obvious change in the telomere length heterogeneity (Figures 3A and S2A), which was affected by Rap1 mutants in overexpression studies (Li and de Lange, 2003).

No Change in the Telomeric Overhang after Rap1 Loss

Removal of Rap1 from several cell lines also did not appear to affect the 3′ telomeric overhang. The amount of ss telomeric DNA was determined by in-gel hybridization of a labeled C-strand telomeric repeat probe to native telomeric restriction fragments. Quantification of normalized ss telomeric DNA signals indicated that Rap1 status had no significant impact on the 3′ overhangs in HT1080, HCT116, and ARPE-19 cells (Figures S2A and S2B).

Unaltered Telomeric Positioning

To determine whether Rap1 is involved in the peripheral positioning of telomeres in newly formed G1 cells (Crabbe et al., 2012), we used mitotic shake-off and analyzed daughter cells in early G1. Using lamin A to mark the nuclear envelope (NE) and FISH to visualize telomeres, the subnuclear position of the telomeric signals was determined and compared between Rap1-proficient and Rap1-deficient cells (Figures 4A and 4B). The distribution of telomeres in the nucleus and median distance from the nuclear envelope was similar for two Rap1-proficient and Rap1-deficient clones in two independent experiments. Moreover, the percentage of telomeres present in a zone defined arbitrarily as the nuclear periphery (within 10% distance from the NE) was also similar regardless of Rap1 status, illustrating that Rap1 is not required for the more peripheral positioning of telomeres in early G1.

Rap1 Affects Transcriptional Regulation, Not Telomeric Chromatin Modification

Mouse Rap1 localizes to over 8,600 gene-associated loci, affecting transcription of numerous genes (Martinez et al.,

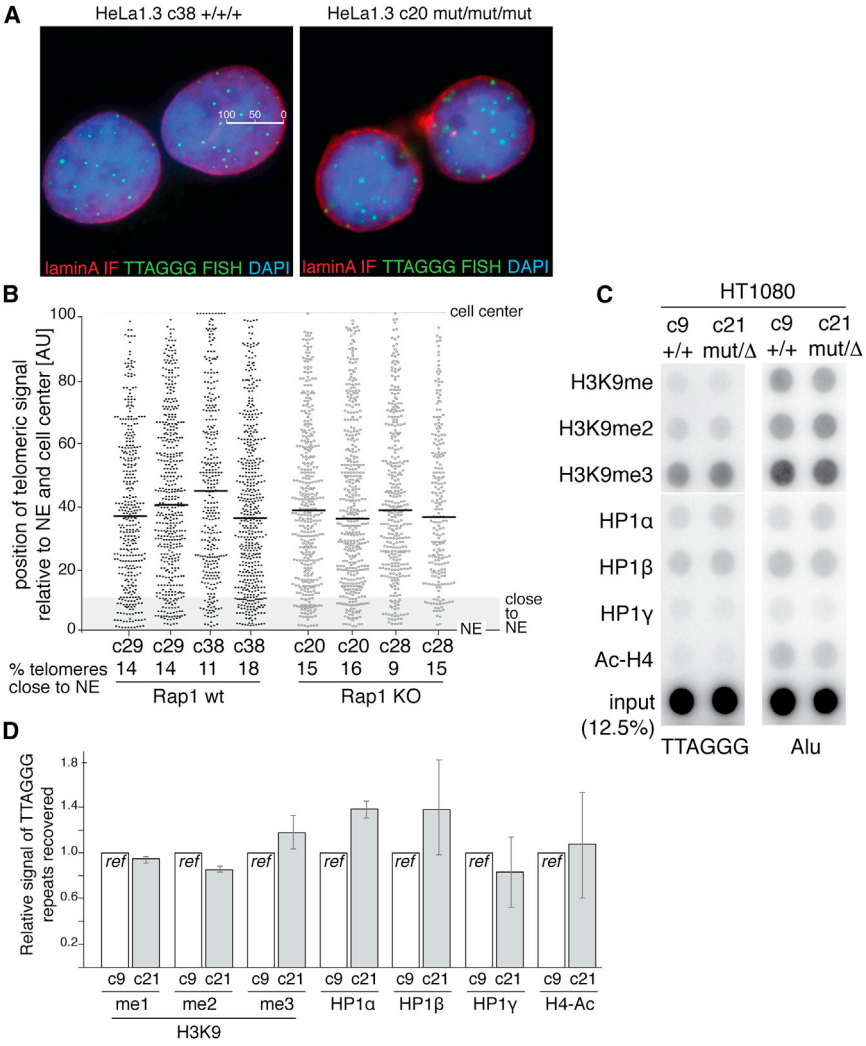

Figure 4. Effects of Rap1 on Telomere Position, Chromatin Modification, and Gene Expression

(A) Combined IF for lamin A (red) and FISH for telomeres (green) in early G1 nuclei of WT and Rap1 KO HeLa1.3 clones. The scale in one nucleus indicates how the position of the telomeric signals was determined. Blue: DAPI DNA stain.

(B) Distance of telomeres from nuclear envelope (NE) in arbitrary units. For each nucleus imaged in a single plane, the ratio between the distance of each telomere from the center and the radius (center to NE) was plotted. Median distance for each clone is indicated by horizontal line. "% telomeres close to NE" reflects telomeres within 10% of the distance from the NE. Two independent experiments for each clone are shown.

(C) ChIP for modified histones at telomeres in WT and Rap1 KO cells. Duplicate blots were probed for telomeric DNA or Alu repeats.

(D) Relative telomeric ChIP signals obtained as in (C) were expressed as the ratio of signal in KO and WT clones (WT set to 1). Values represent averages of two experiments. Error bars represent SEM.

See also Tables S1–S3 and Figure S3.

2010; Yeung et al., 2013; Martínez et al., 2013), while human Rap1 is found at ~63 gene loci (Yang et al., 2011). To query the effect of Rap1 on the transcriptome, we performed microarray profiling on seven Rap1 wild-type (WT) and KO clones derived from three different cell lines: ARPE-19, HT1080, and HCT116. A number of differentially regulated genes were identified (Tables S1–S3). The three Rap1-regulated genes in the ARPE-19 cells (LHX2, LRRC17, and CDO1) were validated by quantitative RT-PCR (qRT-PCR), and their response to Rap1 deletion was further confirmed on an additional ARPE-19 Rap1 KO clone (c26) (Figures S3A–S3C). The Rap1-regulated genes varied between the different cell lines, most likely due to the different origins of the cell lines. Gene ontology analysis was uninformative, because of the low number of genes identified by this limited analysis. However, one Rap1-regulated gene in the HT1080 cells was among the human Rap1-associated loci in the HT1080-derived HTC75 cell line (Yang et al., 2011). Taken together, these data are consistent with a role for Rap1 in transcriptional control in human cells.

Despite the effects of Rap1 on gene expression there was no significant effect of Rap1 on the abundance of the telomeric long noncoding RNA called TERRA (telomeric repeat-containing RNA; reviewed in Feuerhahn et al., 2010) (Figures S3D and S3E). This finding is consistent with the unaltered TERRA levels after deletion of mouse Rap1 (Sfeir et al., 2010). Deletion of human Rap1 also had no detectable effect on general markers for the chromatin status at telomeres, as evidenced by ChIP for methylation of H3K9, acetylation of H4, and HP1α, HP1β, and HP1γ (Figures 4C and 4D).

DISCUSSION

Based on the genetic data presented here, we conclude that human Rap1 is not required for the protection of telomeres from NHEJ and has no obvious effect on telomere length regulation, contrary to what was anticipated from other studies (Bae and Baumann, 2007; Sarthy et al., 2009; Li and de Lange, 2003; O'Connor et al., 2004). In addition, telomeres lacking Rap1 remained protected from DNA damage signaling and HDR and had a normal 3′ overhang. These findings are in agreement with the mouse Rap1 KO, which revealed no obvious phenotype other than that of telomeres becoming prone to undergo HDR when Ku70/80 was absent (Sfeir et al., 2010). Whether human telomeres lacking Rap1 also recombine more readily in a Ku70/80-deficient setting is difficult to assess, since deletion of human Ku70/80 leads to rapid telomere loss and cell death (Li et al., 2002; Wang et al., 2009).

Despite this lack of requirement for Rap1 at telomeres, the human gene encoding Rap1 has diverged little from its chimpanzee counterpart (1 base change/100 codons; 0.25 aa changes/100 aa), whereas the genes for other shelterin components show much greater divergence (e.g., 3.6, 2.4, and 1.7 base changes/100 codons and 2.2, 1.1, and 0.65 aa changes/100 aa for TRF2, TRF1, and TIN2, respectively). Furthermore, assessment of a gene damage index for all protein-coding genes places *TERF2IP* in the top 20% of human genes with regard to mutation intolerance (Y. Itan, personal communication). In addition, Rap1 ranks among the top 10% of human genes in terms of "functional indispensability," a characteristic that incorporates gene centrality (based on interaction data pooled from various biological systems), structural information, and evolutionary constraints (Khurana et al., 2013). In this regard, only TIN2 scores higher than Rap1, as expected based on its multiple interaction interfaces in shelterin.

These results raise the question why Rap1 is conserved. It appears unlikely that protection of telomeres from HDR is its sole raison d'ètre, given the additional repression by Ku70/80. Furthermore, it seems unlikely that Rap1 has a tissue-specific role at telomeres, given that mice lacking Rap1 are alive and largely normal and the lack of telomeric phenotypes upon Rap1 deletion from four human cell lines of different tissue origin. The conservation of Rap1 is also not explained by a role in meiosis, since the Rap1 KO mice are fertile and, unlike yeast lacking Rap1, form a normal meiotic bouquet (Kanoh and Ishikawa, 2001; Chikashige and Hiraoka, 2001; Chikashige et al., 2006; Sfeir et al., 2010; Scherthan et al., 2011; Shibuya et al., 2014). It is not excluded that Rap1, like TIN2, has (as yet unknown) multiple interactions within shelterin or interacts with shelterin-associated factors that explain its conservation or that its role at telomeres is redundant. However, we favor the idea that the conservation of Rap1 is due to its role in transcriptional regulation, where it may have multiple distinct interaction partners that constrain its evolution. It will be of interest to identify the Rap1-interacting partners that are at gene loci, since such partners may well be used by Rap1 to fulfill (as yet undefined) telomere functions.

Our data point to the difficulty in interpreting experiments in which telomeric phenotypes are observed upon overexpression of shelterin (mutant) proteins or their partial inactivation by shRNAs. We suspect that the prior finding of changes in telomere length and heterogeneity upon overexpression of Rap1 mutants (Li and de Lange, 2003) were due to nucleoplasmic titration of factors that (indirectly) influence these phenotypes. Similarly, the artificial tethering of Rap1 to telomeres may have had an effect on NHEJ that does not reflect the normal function of the protein (Sarthy et al., 2009).

These data indicate that while mammalian Rap1 has functionally diverged away from its yeast predecessors, mouse and human Rap1 are very similar. Both Rap1 KO mice and human cells are viable, lack hallmarks of telomere dysfunction, and have no overt change in telomere length settings. While the Rap1 components of human and mouse shelterin are indistinguishable, it will be important to query the functions of other shelterin components and associated factors to gain a complete understanding of telomere maintenance and protection in human cells. Our data show that genetic approaches, such as the use of TALENs and CRISPR (Hsu et al., 2014), are versatile tools to this effect.

EXPERIMENTAL PROCEDURES

Detailed experimental procedures are available in Supplemental Experimental Procedures. Cell culture techniques, telomere length analysis, telomeric overhang assay, analysis of metaphase spreads, TIF analysis, ChIP, telomeric FISH, immunofluorescence, and immunoblotting analysis were performed as described previously (Sfeir et al., 2010; Takai et al., 2010). TALENs KO of *TERF2IP* was performed using standard protocols (Chen et al., 2011). The assay for telomeric position was published previously (Crabbe et al., 2012). Microarray analysis was performed using Whole Human Genome DNA microarrays (Illumina HumanHT-12 v4) with GeneSpring v12.6 for data analysis.

ACCESSION NUMBERS

Microarray data have been deposited in the Gene Expression Omnibus under the accession number GSE61900.

SUPPLEMENTAL INFORMATION

Supplemental Information includes Supplemental Experimental Procedures, three figures, and three tables and can be found with this article online at http://dx.doi.org/10.1016/j.celrep.2014.10.014.

AUTHOR CONTRIBUTIONS

All experiments were designed by S.K. and T.d.L. and executed by S.K. D.H. designed the TALENs and provided advice. S.K. and T.d.L. wrote the paper.

ACKNOWLEDGMENTS

We thank Dr. Alexandre Bolze for his guidance on the evolutionary selection pressure on Rap1. We thank Dr. Agnel Sfeir for helpful discussion. This work was supported by grants from the NIH (5R37GM49046 and 5RO1AG16642) to T.d.L. T.d.L. is an American Cancer Society Research Professor. D.H. is a New Scholar in Aging of the Ellison Medical Foundation and supported by the Glenn Foundation as well as the Shurl and Kay Curci Foundation.

Received: June 30, 2014
Revised: September 2, 2014
Accepted: October 3, 2014
Published: November 6, 2014

REFERENCES

Bae, N.S., and Baumann, P. (2007). A RAP1/TRF2 complex inhibits nonhomologous end-joining at human telomeric DNA ends. Mol. Cell *26*, 323–334.

Chen, F., Pruett-Miller, S.M., Huang, Y., Gjoka, M., Duda, K., Taunton, J., Collingwood, T.N., Frodin, M., and Davis, G.D. (2011). High-frequency genome editing using ssDNA oligonucleotides with zinc-finger nucleases. Nat. Methods *8*, 753–755.

Chikashige, Y., and Hiraoka, Y. (2001). Telomere binding of the Rap1 protein is required for meiosis in fission yeast. Curr. Biol. *11*, 1618–1623.

Chikashige, Y., Tsutsumi, C., Yamane, M., Okamasa, K., Haraguchi, T., and Hiraoka, Y. (2006). Meiotic proteins bqt1 and bqt2 tether telomeres to form the bouquet arrangement of chromosomes. Cell *125*, 59–69.

Cockell, M., Palladino, F., Laroche, T., Kyrion, G., Liu, C., Lustig, A.J., and Gasser, S.M. (1995). The carboxy termini of Sir4 and Rap1 affect Sir3 localization: evidence for a multicomponent complex required for yeast telomeric silencing. J. Cell Biol. *129*, 909–924.

Conrad, M.N., Wright, J.H., Wolf, A.J., and Zakian, V.A. (1990). RAP1 protein interacts with yeast telomeres in vivo: overproduction alters telomere structure and decreases chromosome stability. Cell *63*, 739–750.

Crabbe, L., Cesare, A.J., Kasuboski, J.M., Fitzpatrick, J.A., and Karlseder, J. (2012). Human telomeres are tethered to the nuclear envelope during postmitotic nuclear assembly. Cell Reports *2*, 1521–1529.

Feuerhahn, S., Iglesias, N., Panza, A., Porro, A., and Lingner, J. (2010). TERRA biogenesis, turnover and implications for function. FEBS Lett. *584*, 3812–3818.

Hardy, C.F., Sussel, L., and Shore, D. (1992a). A RAP1-interacting protein involved in transcriptional silencing and telomere length regulation. Genes Dev. *6*, 801–814.

Hardy, C.F., Balderes, D., and Shore, D. (1992b). Dissection of a carboxy-terminal region of the yeast regulatory protein RAP1 with effects on both transcriptional activation and silencing. Mol. Cell. Biol. *12*, 1209–1217.

Hsu, P.D., Lander, E.S., and Zhang, F. (2014). Development and applications of CRISPR-Cas9 for genome engineering. Cell *157*, 1262–1278.

Kanoh, J., and Ishikawa, F. (2001). spRap1 and spRif1, recruited to telomeres by Taz1, are essential for telomere function in fission yeast. Curr. Biol. *11*, 1624–1630.

Khurana, E., Fu, Y., Chen, J., and Gerstein, M. (2013). Interpretation of genomic variants using a unified biological network approach. PLoS Comput. Biol. *9*, e1002886.

Konig, P., Giraldo, R., Chapman, L., and Rhodes, D. (1996). The crystal structure of the DNA-binding domain of yeast RAP1 in complex with telomeric DNA. Cell *85*, 125–136.

Kyrion, G., Boakye, K.A., and Lustig, A.J. (1992). C-terminal truncation of RAP1 results in the deregulation of telomere size, stability, and function in Saccharomyces cerevisiae. Mol. Cell. Biol. *12*, 5159–5173.

Levy, D.L., and Blackburn, E.H. (2004). Counting of Rif1p and Rif2p on Saccharomyces cerevisiae telomeres regulates telomere length. Mol. Cell. Biol. *24*, 10857–10867.

Li, B., and de Lange, T. (2003). Rap1 affects the length and heterogeneity of human telomeres. Mol. Biol. Cell *14*, 5060–5068.

Li, B., Oestreich, S., and de Lange, T. (2000). Identification of human Rap1: implications for telomere evolution. Cell *101*, 471–483.

Li, G., Nelsen, C., and Hendrickson, E.A. (2002). Ku86 is essential in human somatic cells. Proc. Natl. Acad. Sci. USA *99*, 832–837.

Lickwar, C.R., Mueller, F., Hanlon, S.E., McNally, J.G., and Lieb, J.D. (2012). Genome-wide protein-DNA binding dynamics suggest a molecular clutch for transcription factor function. Nature *484*, 251–255.

Liu, C., and Lustig, A.J. (1996). Genetic analysis of Rap1p/Sir3p interactions in telomeric and HML silencing in Saccharomyces cerevisiae. Genetics *143*, 81–93.

Lustig, A.J., Kurtz, S., and Shore, D. (1990). Involvement of the silencer and UAS binding protein RAP1 in regulation of telomere length. Science *250*, 549–553.

Martinez, P., Thanasoula, M., Carlos, A.R., Gómez-López, G., Tejera, A.M., Schoeftner, S., Dominguez, O., Pisano, D.G., Tarsounas, M., and Blasco, M.A. (2010). Mammalian Rap1 controls telomere function and gene expression through binding to telomeric and extratelomeric sites. Nat. Cell Biol. *12*, 768–780.

Martínez, P., Gómez-López, G., García, F., Mercken, E., Mitchell, S., Flores, J.M., de Cabo, R., and Blasco, M.A. (2013). RAP1 protects from obesity through its extratelomeric role regulating gene expression. Cell Reports *3*, 2059–2074.

Miller, K.M., Ferreira, M.G., and Cooper, J.P. (2005). Taz1, Rap1 and Rif1 act both interdependently and independently to maintain telomeres. EMBO J. *24*, 3128–3135.

O'Connor, M.S., Safari, A., Liu, D., Qin, J., and Songyang, Z. (2004). The human Rap1 protein complex and modulation of telomere length. J. Biol. Chem. *279*, 28585–28591.

Palm, W., and de Lange, T. (2008). How shelterin protects mammalian telomeres. Annu. Rev. Genet. *42*, 301–334.

Pardo, B., and Marcand, S. (2005). Rap1 prevents telomere fusions by nonhomologous end joining. EMBO J. *24*, 3117–3127.

Sarthy, J., Bae, N.S., Scrafford, J., and Baumann, P. (2009). Human RAP1 inhibits non-homologous end joining at telomeres. EMBO J. *28*, 3390–3399.

Scherthan, H., Sfeir, A., and de Lange, T. (2011). Rap1-independent telomere attachment and bouquet formation in mammalian meiosis. Chromosoma *120*, 151–157.

Sedivy, J., Vogelstein, B., Liber, H., Hendrickson, E.A., and Rosmarin, A. (1999). Gene targeting in human cells without isogenic DNA. Science *283*, 9–9a.

Sfeir, A., Kabir, S., van Overbeek, M., Celli, G.B., and de Lange, T. (2010). Loss of Rap1 induces telomere recombination in the absence of NHEJ or a DNA damage signal. Science *327*, 1657–1661.

Shibuya, H., Ishiguro, K., and Watanabe, Y. (2014). The TRF1-binding protein TERB1 promotes chromosome movement and telomere rigidity in meiosis. Nat. Cell Biol. *16*, 145–156.

Shore, D. (1994). RAP1: a protean regulator in yeast. Trends Genet. *10*, 408–412.

Shore, D., and Nasmyth, K. (1987). Purification and cloning of a DNA binding protein from yeast that binds to both silencer and activator elements. Cell *51*, 721–732.

Silverman, J., Takai, H., Buonomo, S.B., Eisenhaber, F., and de Lange, T. (2004). Human Rif1, ortholog of a yeast telomeric protein, is regulated by ATM and 53BP1 and functions in the S-phase checkpoint. Genes Dev. *18*, 2108–2119.

Sussel, L., and Shore, D. (1991). Separation of transcriptional activation and silencing functions of the RAP1-encoded repressor/activator protein 1: isolation of viable mutants affecting both silencing and telomere length. Proc. Natl. Acad. Sci. USA *88*, 7749–7753.

Takai, K.K., Hooper, S., Blackwood, S., Gandhi, R., and de Lange, T. (2010). In vivo stoichiometry of shelterin components. J. Biol. Chem. *285*, 1457–1467.

Teixeira, M.T., Arneric, M., Sperisen, P., and Lingner, J. (2004). Telomere length homeostasis is achieved via a switch between telomerase- extendible and -nonextendible states. Cell *117*, 323–335.

Urnov, F.D., Rebar, E.J., Holmes, M.C., Zhang, H.S., and Gregory, P.D. (2010). Genome editing with engineered zinc finger nucleases. Nat. Rev. Genet. *11*, 636–646.

Wang, Y., Ghosh, G., and Hendrickson, E.A. (2009). Ku86 represses lethal telomere deletion events in human somatic cells. Proc. Natl. Acad. Sci. USA *106*, 12430–12435.

Wotton, D., and Shore, D. (1997). A novel Rap1p-interacting factor, Rif2p, cooperates with Rif1p to regulate telomere length in Saccharomyces cerevisiae. Genes Dev. *11*, 748–760.

Xu, L., and Blackburn, E.H. (2004). Human Rif1 protein binds aberrant telomeres and aligns along anaphase midzone microtubules. J. Cell Biol. *167*, 819–830.

Yang, X., Figueiredo, L.M., Espinal, A., Okubo, E., and Li, B. (2009). RAP1 is essential for silencing telomeric variant surface glycoprotein genes in Trypanosoma brucei. Cell *137*, 99–109.

Yang, D., Xiong, Y., Kim, H., He, Q., Li, Y., Chen, R., and Songyang, Z. (2011). Human telomeric proteins occupy selective interstitial sites. Cell Res. *21*, 1013–1027.

Yeung, F., Ramírez, C.M., Mateos-Gomez, P.A., Pinzaru, A., Ceccarini, G., Kabir, S., Fernández-Hernando, C., and Sfeir, A. (2013). Nontelomeric role for Rap1 in regulating metabolism and protecting against obesity. Cell Reports *3*, 1847–1856.

Cell Reports, Volume *9*

Supplemental Information

TALEN Gene Knockouts Reveal No Requirement for the Conserved Human Shelterin Protein Rap1 in Telomere Protection and Length Regulation

Shaheen Kabir, Dirk Hockemeyer, and Titia de Lange

Figure S1. Kabir et al.

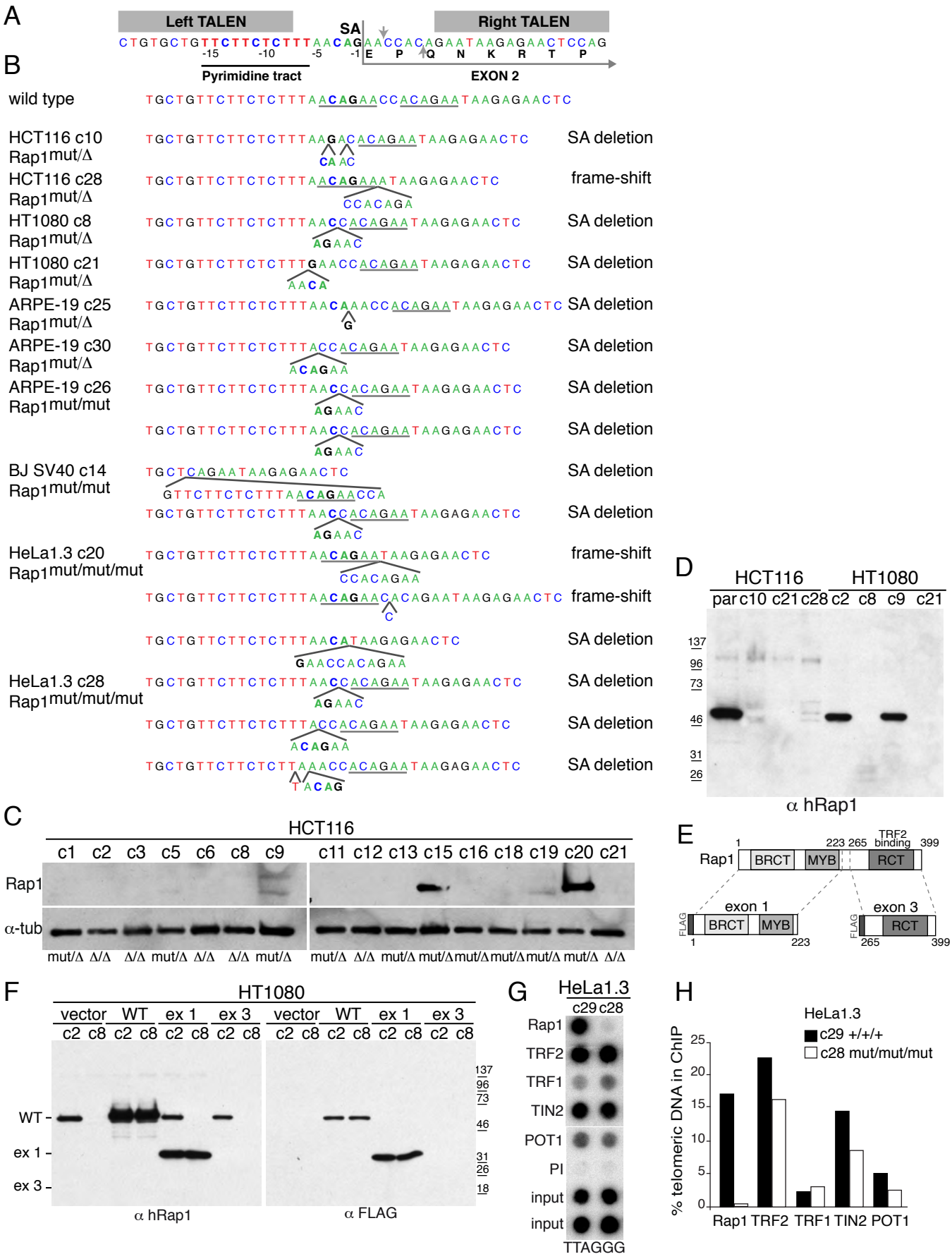

Figure S2. Kabir et al.

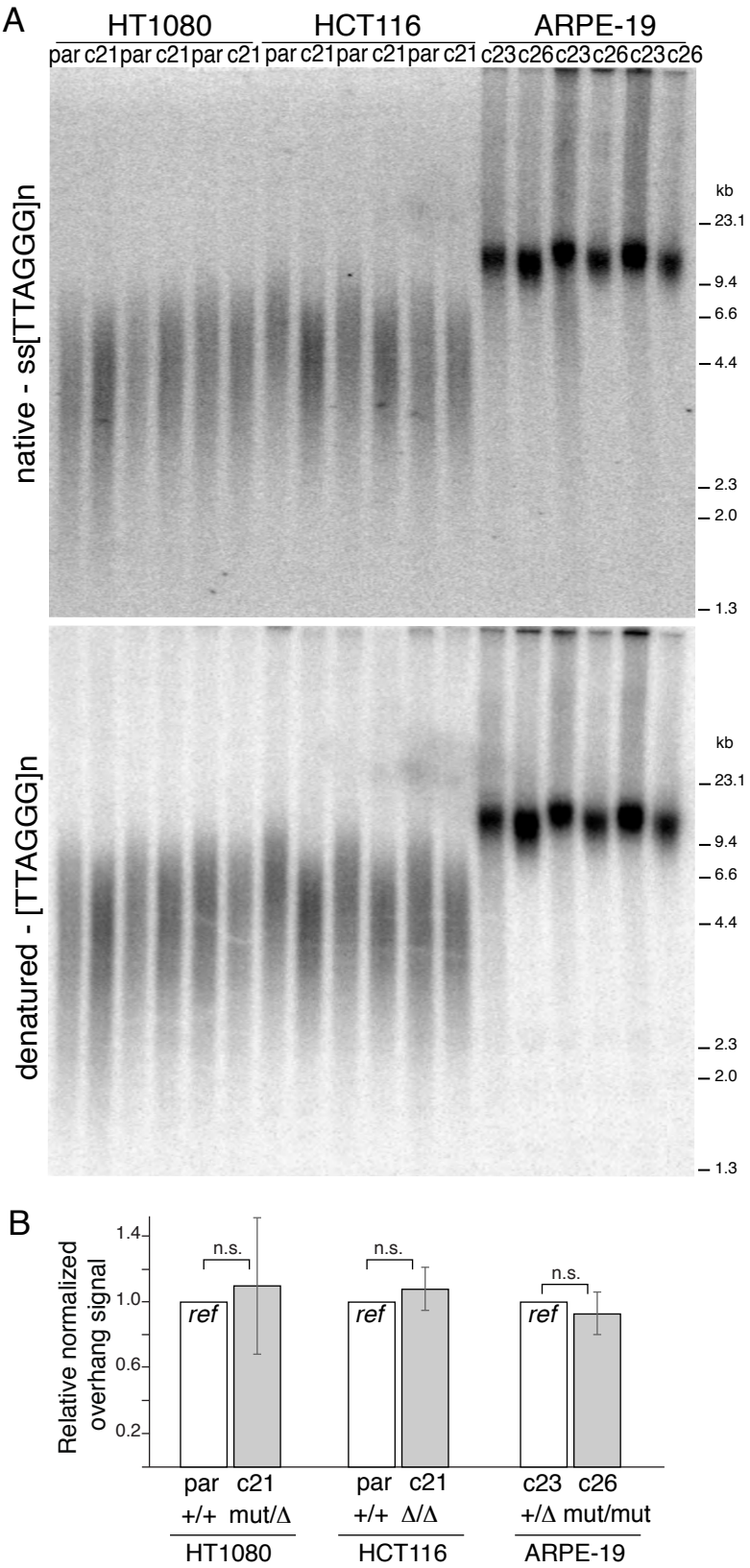

Figure S3. Kabir et al.

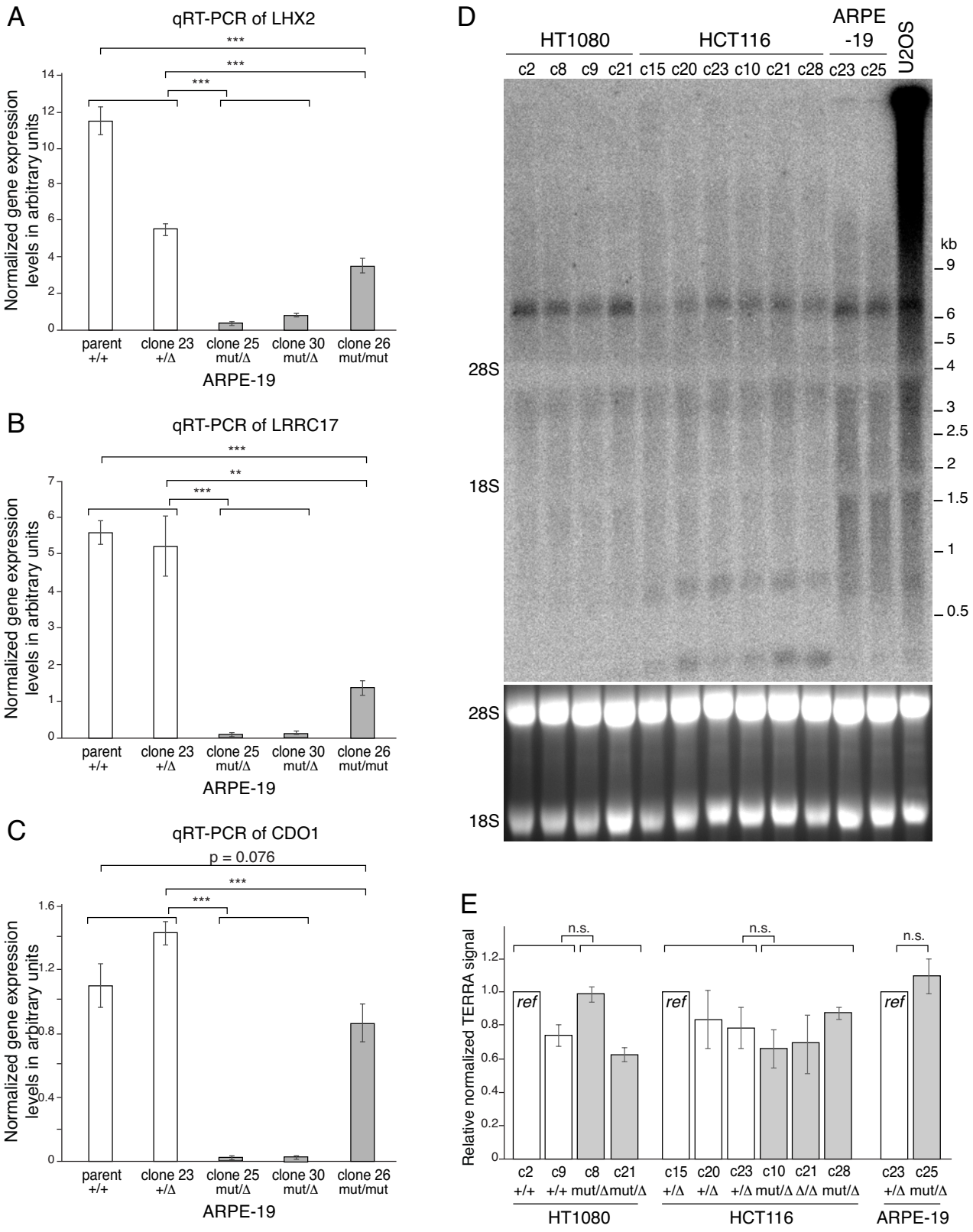

Supplemental Information

Supplemental Figures and Figure Legends

Figure S1, Related to Figure 1.

TALEN-induced mutations in the *TERF2IP* locus.

(A) Schematic illustrating TALEN binding sites, their predicted cutting site (grey arrows), the pyrimidine tract, splice acceptor (SA), and the location of exon 2 in the *TERF2IP* locus. A short repeat (underlined in grey) is frequently mutated in the mutant alleles.

(B) Relevant sequences of the indicated clones. Predicted consequences of the mutations are indicated on the right.

(C) Immunoblotting of protein from targeted homozygous and heterozygous HCT116 clones showing absence of Rap1 in a large proportion of heterozygous clones. Genotypes indicated below.

(D) Immunoblots of HCT116 and HT1080 KO clones probed with anti-hRap1 showing the absence of detectable truncated Rap1 proteins.

(E) Schematic of retroviral constructs expressing FLAG-tagged exon 1 (ex 1) and FLAG-tagged exon 3 (ex 3).

(F) Immunoblotting for the expression of constructs in (E) in HT1080 KO and WT clones. The protein fragment encoded by exon 1 is expressed and detected by the Rap1 antibody. The protein fragment encoded by exon 3 contains epitopes that the Rap1 antibody can recognize, but lack of detectable signal indicates that it is not expressed.

(G) Telomeric ChIP of HeLa 1.3 WT and KO cells.

(H) Quantification of the percent of telomeric DNA recovered in each ChIP. Methods as in Figure 1D and E.

Figure S2, Related to Figure 3.

No change in the telomeric overhangs upon Rap1 loss.

(A) Telomeric DNA analysis of WT and KO clones in three different cell lines. Top, in-gel detection of native telomeric restriction fragments with a C-strand telomeric probe revealing the G-strand overhang signals; bottom, same gel rehybridized after in situ denaturation of the DNA, revealing the total telomeric DNA in each lane. Three biological replicates of each cell line were run adjacent to each other on the same gel.

(B) Overhang signals were normalized to total telomeric signals in each lane and plotted as a ratio compared to the WT overhang signal of the corresponding cell line. Error bars represent SDs. Lack of statistical significance derived from two-tailed paired t-tests using the three independent experiments conducted with each cell line.

Figure S3, Related to Figure 4.

Validation of Rap1 as a transcriptional regulator, but not of TERRA.

(A-C) Quantitative RT-PCR illustrates differential expression of three genes ((A) LHX2, (B) LRRC17, (C) CDO1) in Rap1 WT and KO ARPE-19 cells. Gene expression was normalized to GAPDH and mean expression level for each gene as determined by the ΔCt method from 3 independent replicates is graphed in arbitrary units. Error bars represent SDs. Significance was calculated by two-tailed unpaired T-Tests. *** indicates $p \leq 0.001$.

(D) Northern blot hybridized with a telomeric probe (Sty11) showing TERRA levels of Rap1 WT and KO clones in the HT1080, HCT116 and ARPE-19 cell lines. U2OS serves as a positive control for TERRA expression. Ethidium bromide staining of ribosomal RNA serves as a loading control.

(E) TERRA signals were normalized using the 18S ribosomal RNA and plotted as a ratio compared to the WT TERRA signal of the corresponding cell line. Error bars represent SDs. Two-tailed unpaired t-tests of 3 independent experiments illustrates lack of statistical significance between Rap1 WT and KO TERRA expression levels.

Table S1. Microarray expression analysis for ARPE-19, related to Figure 4.

Cell Line	Gene (chromosome) [LogFC][a]		
KO v WT	LHX2 (chr9)	LRRC17 (chr7)	CDO1 (chr5)
c25 v c23	-3.3	-5.1, -3.4	-3.5
c30 v c23	-2.7	-5.1, -3.4	-3.8
c25 v par	-4.2	-4.6, -3.1	-3.3
c30 v par	-3.7	-4.5, -3.0	-3.5

[a],Multiple LogFC values reflect data from multiple probes for the corresponding gene.

Table S2. Microarray expression analysis for HT1080, related to Figure 4.

Cell Line	Gene (chromosome) [LogFC][a]							
KO v WT	ATP9A (chr20)	CDCP1[b] (chr3)	CYP2J2 (chr1)	FAIM3 (chr1)	MGC 39900	NELL2 (chr12)	PTGR1 (chr9)	TERF2IP (chr16)
c8 v c2	3.0	3.4, 1.8, 2.5, -	2.0	-3.4	-2.1	3.0	2.0, 1.7	-2.9
c21 v c2	3.1	3.7, 1.9, 2.4, 3.0	2.2	-3.6	-2.3	2.2	2.1, 1.9	-2.3
c8 v c9	3.8	3.6, 1.8, 2.3, -	1.6	-2.0	-2.7	2.9	2.0, 1.7	-2.9
c21 v c9	3.9	3.9, 1.8, 2.3, 2.8	3.5	-2.2	-2.9	2.2	2.1, 1.9	-2.3

[a],Multiple LogFC values reflect data from multiple probes for the corresponding gene. [b] CDCP1 was identified as a Rap1 associated locus by ChIP-seq in a subclone of HT1080 (Yang et al., 2011).

Table S3. Microarray expression analysis for HCT116, related to Figure 4.

Cell Line	Gene (chromosome) [LogFC] [a]		
KO v WT	BMP4 (chr14)	SLC2A3 (chr12)	SUSD2 (chr22)
c10 v c15	-2.0	-3.4	-2.6
c21 v c15	-2.1	-2.7	-2.2
c28 v c15	-1.9	-2.3	-2.1
c10 v c20	-2.0	-2.7	-2.0
c21 v c20	-2.0, -2.5	-2.0	-1.6
c28 v c20	-1.8	-1.5	-1.5
c10 v c23	-1.8	-2.9	-2.8
c21 v c23	-1.9, -2.4	-2.1	-2.5
c28 v c23	-1.7	-1.7	-2.3

[a],Multiple LogFC values reflect data from multiple probes for the corresponding gene.

Supplemental Experimental Procedures

TALENs and *TERF2IP* Targeting Construct

The heterodimeric TALEN pair for *TERF2IP* targeting was constructed using the following RVD sequences. LEFT2: 5'-HD-NG-NN-NG-NN-HD-NG-NN-NG-NG-HD-NG-NG-HD-NG-HD-NG, RIGHT1: 5'-HD-NG-NN-NN-NI-NN-NG-NG-HD-NG-HD-NG-NG-NI-NG-NG-3'. The PGK Neomycin cassette from the PL451 vector (NCI) was liberated using restriction enzymes *Nhe*I (5') and *Bst*BI (3') and ligated into *Nhe*I- and *Bst*BI- digested pSL301 (cloning vector from Invitrogen). The pEF Blasticidin cassette from plasmid pEF/Bsd (Life Technologies) was released using *Nhe*I (5') and *Eco*RI (3') and ligated into *Nhe*I- and *Eco*RI- digested pSL301. The 5' and 3' homology arms were PCR-amplified with restriction site overhangs from genomic SV40LT BJ fibroblast DNA. Primers for PCR of the 5' arm were as follows: 5'-ATGCGGTACCTTGCCCAAACTCCTGTCTTCTTAGGGC-3' and 5'-GCATGCTAGCAGAGAAGAACAGCACAGATTAGCAATAGCC-3'. Primers for PCR of the 3' arm were 5'-ATGCTTCGAACTAGATTTACTCATTATTTTTTTCCCTACC-3' and 5'-GCATTTCGAACCTGTAATCCCAGCACTTTGGGAG-3'. The resulting 600 bp 5' homology arm ends 7 bp from the intron 1/exon 2 junction and has *Kpn*I and *Nhe*I sites on the 5' and 3' ends, respectively. The resulting 578 bp 3' homology arm starts 32 bp from the exon 2/intron 2 junction and has *Bst*BI restriction sites at both ends. The homology arms were cloned into the relevant restriction sites in pSL301 containing either the PGK Neomycin or pEF Blasticidin. The 3' homology arm insertion was screened for orientation and the donor constructs were sequenced using the following primers: T7, T3, 5'-GCTCGCGTCGTGCAGGACGT-3' (PGK internal primer), and 5'- GCTGTGCTCGACGTTGTCAC-3' (Neomycin internal primer).

Cell Culture

HCT116, HT1080, ARPE-19, and HeLa1.3 cells were grown in Dulbecco modified Eagle medium (DMEM) supplemented with L-glutamine, penicillin-streptomycin, nonessential amino acids and 15% bovine calf serum (BCS) (HyClone). SV40-large T transformed BJ fibroblasts (neo resistant) were cultured in complete DMEM containing 199 medium (4:1) and 10% BCS.

***TERF2IP* Targeting and Cell cloning**

All cell lines were transfected in 10 cm dishes at a density of $3x10^6$ cells using Lipofectamine 2000 (Life Technologies) with 4 μg of each TALEN construct and 20 μg of the donor construct. 48 hours after transfection, all cell lines, except for HeLa1.3, were plated in selection medium in 10 cm plates at varying densities ranging from 3,900 to 500,000 cells (using two-fold dilutions). HeLa1.3 cells were plated in 10 cm dishes using two-fold dilutions starting from 8000 cells down to 75 cells. G418 was used at 1 mg/ml to select neomycin-resistant HCT116 cells, at 900 μg/ml for HT1080 cells, and at 800 μg/ml for ARPE-19 cells. Blasticidin was used at 5 μg/ml for HeLa1.3 selection and at 2.5 μg/ml for SV40LT BJ selection. Clones emerged at a frequency of approximately 1 clone per 500 plated HCT116 cells, 1 clone per 2,600 plated HT1080 cells, 1 clone per 7,800 plated ARPE-19 cells, 1 clone per 125 plated HeLa1.3 cells, and 1 clone per 62,500 plated SV40LT BJ cells. The media was not changed after initial plating. Clones were picked 12 days later for all cell lines except the SV40LT BJ clones, which were picked 3 weeks after plating. Approximately 60-70 clones were picked for each cell line using cloning cylinders from plates that contained well-spaced clones and the cells were transferred into 24 well plates. After reaching confluence, half of the cells in each well were harvested to extract genomic DNA, while the remaining cells were expanded into 6 well plates. Approximately 30-40 clones were screened per cell line.

Genotyping and Sequencing

Genotyping PCR used the following primers: F1: 5'- GTGGATTGTGGTACGT GGCCCAGATCTGCC-3'; R1: 5'-TAACATACCACAACCTCCTCAAACTCCCGG-3'; R2: 5'-CATCTGCACGAGACTAGTGAGACGTGCTAC-3'. PCR was performed in 25 μl containing 50 ng of DNA, 0.2 μM of each primer, 0.1 μM dNTPs, 1.5 mM $MgCl_2$, 50 mM KCl, 10 mM Tris-HCl pH 8.0, and 0.5 U of TaKaRa Taq polymerase. Conditions were as follows: 95°C for 4 min, 25 cycles of 95°C for 30 sec, 62°C for 30 sec, 72°C for 45 sec and final extension at 72°C for 5 min. Clones identified as heterozygous by PCR genotyping and southern blotting but lacking Rap1 protein on western blots were sequenced by PCR amplifying the remaining 'WT' allele with primers F1 and R1 using the PCR conditions described above. The PCR products were eluted from agarose gels and sequenced with primers F1 and R1. The relevant *TERF2IP* PCR product from clones that lacked detectable Rap1 protein but appeared to be untargeted (homozygous 'WT') according to PCR genotyping and southern blotting were PCR amplified using primers F1 and R1, gel-eluted and cloned by TA cloning (Life Technologies). A minimum of 8 resulting TA clones per cell line were sequenced to identify mutations in both alleles. The latter procedure was applied to clones from the ARPE-19, SV40LT BJ, and HeLa1.3 cell lines.

Immunoblotting

Immunoblotting was performed as previously described (Takai et al., 2010). Briefly, cells were harvested by trypsinization, resuspended in Laemmli buffer (100mM Tris-HCl pH 6.8, 200 mM DTT, 3% SDS, 20% glycerol, 0.05% bromophenol blue) at 10,000 cells per μl, denatured for 5 min at 95°C, sheared with an insulin needle, and resolved on SDS/PAGE gels using 100,000 cells per lane. Blots were blocked in 5% non-fat dry milk/PBS+0.1% Tween20. Antibodies used were as follows: Rap1 (765, rabbit polyclonal); alpha-tubulin (Sigma T9026). The hRap1 Ab was generated using full-length hRap1 recombinant protein as an antigen and reacts with multiple Rap1 domains.

Telomeric ChIP

Telomeric ChIP was conducted as previously described (Loayza and de Lange, 2003). The following antibodies or crude sera were used: Rap1 (765, rabbit polyclonal); TRF2 (647, rabbit polyclonal); TRF1 (371, rabbit polyclonal); TIN2 (864, rabbit polyclonal); POT1 (Abcam ab124784); TPP1 (1151; rabbit polyclonal); H3K9me1 (Abcam ab9045); H3K9me2 (Abcam ab1220); H3K9me3 (Abcam ab8898); HP1alpha (Abcam ab77256); HP1beta (Abcam ab10478); HP1gamma (Abcam ab10480); Acetyl Histone H4 (Millipore 06-598).

IF-FISH

IF-FISH was conducted as previously described (Dimitrova and de Lange, 2006). Briefly, cells grown on coverslips were fixed for 10 min in 2% paraformaldehyde/3% sucrose at room temperature, followed by three 5 min PBS washes. Coverslips were incubated in blocking solution (1 mg/ml BSA, 3% goat serum, 0.1% TritonX-100, 1 mM EDTA in PBS) for 30 min, followed by incubation with primary antibodies diluted in blocking solution for 1 h at rt. Primary antibodies used were: 53BP1 (Novus 100-304) and Lamin A (Sigma L1293). Cells were washed three times for 5 min with PBS and then incubated with secondary antibodies diluted in blocking solution for 30 min at rt. The secondary antibody used was RRX-anti-rabbit (Jackson 711-295-152). Coverslips were dehydrated with 70%, 95% and 100% ethanol and allowed to dry. Hybridizing solution (70% formamide, 0.5% blocking reagent from Roche, 10 mM Tris-HCl pH 7.2, FITC-OO-(CCCTAA)3 PNA probe from Applied Biosystems) was added to each coverslip and denatured at 80ºC for 5 min, followed by a 2 h incubation at rt. Two 15-min washes in 70% formamide/10 mM Tris-HCl pH 7.2 and three 5-min washes with PBS were performed. DNA was stained with DAPI in the PBS washes and coverslips were mounted using antifade reagent ProLong Gold from Life Technologies. Images were captured using a Zeiss AxioPlan II microscope with a Hamamatsu C4742-95 camera using Volocity software from Perkin Elmer. Distances of telomeres from nuclear membrane were calculated using Image J software.

Telomeric FISH and CO-FISH

Telomeric FISH and CO-FISH were conducted as previously described (van Steensel et al., 1998; Celli et al., 2006). Briefly, colcemid was added to cells 2 hours prior to harvest. Cells were collected by trypsinization, swollen in 0.075 M KCl and fixed overnight at 4ºC in methanol:acetic acid (3:1). Metaphase spreads were dropped on glass slides and aged overnight. Slides were hybridized with FITC-OO-$[CCCTAA]_3$ PNA probe in hybridizing solution, denatured at 80ºC for 5 min and incubated for 2 h at rt. Two 15-min washes in 70% formamide/10 mM Tris-HCl pH 7.2 and three 5 min washes with 0.1 M Tris-HCl pH 7.2/0.15 M NaCl/0.08% Tween20 were performed. DAPI was added to last wash for DNA stain. Slides were dehydrated in 70%, 95%, and 100% ethanol and mounted using ProLong Gold antifade from Life Technologies. Images were captured using a Zeiss AxioPlan II microscope with a Hamamatsu C4742-95 camera using Volocity software from Perkin Elmer. For CO-FISH, BrdU:BrdC (3:1) was added 14 h prior to harvest. Harvesting and metaphase conditions were as described for FISH. Slides were treated with 0.5 mg/ml RNase A diluted in PBS, stained with 0.5 μg/ml Hoechst 33258, exposed to 5400J/m^2 of UV light and subsequently digested with 800 U of Exonuclease III from Promega for 10 min at room temperature. Slides were rinsed with PBS, dehydrated with 70%, 95% and 100% ethanol and sequentially hybridized with TAMRA-OO-$[TTAGGG]_3$ and FITC-OO-$[CCCTAA]_3$ for 2 h each at rt, without denaturation. Washing, mounting and capture conditions were as described for FISH.

Genomic Blotting, Telomere Overhang and Telomere Length Analysis

Cells were harvested by trypsinization, washed with PBS, and either pelleted and frozen at -80ºC (for telomere length analysis) or processed immediately (for genotyping and telomere overhang analysis) for genomic DNA collection. Genomic DNA was extracted as previously described (de Lange et al., 1990). DNA for genotyping was digested with *EcoR*I, quantitated by fluorometry using Hoechst 33258 and 10 μg was loaded on a 0.7% agarose gel run in 0.5X

TBE. DNA for telomere overhang and length analysis was digested with *Mbo*I and *Alu*I, quantified using Hoechst, and 1 μg was run on 0.7% agarose gels in 0.5X TBE. For genomic blots used for genotyping and telomere length analysis, the gels were depurinated with 0.5N HCl, denatured and neutralized using standard Southern blotting procedures and transferred as previously described (de Lange et al., 1990). Blots were probed with a *TERF2IP* 5' arm probe (indicated in Fig. 1a, Klenow-labeled using random primers and α-^{32}P-dCTP) or a Sty11 probe (de Lange, 1992) for genotyping and telomere length analysis, respectively. For telomere overhang analysis, gels were dried and probed with a [CCCTAA]4 end-labeled with Polynucleotide kinase and γ-^{32}P-ATP as previously described (Karlseder et al., 2002). Gels and membranes were exposed to PhosphorImager screens and quantified with ImageQuant software.

Northern Analysis for TERRA

Total RNA was prepared using RNeasy Mini Spin columns (QIAGEN) according to the manufacturer's instructions and northern blot analysis was performed as previously described (Azzalin et al., 2007). Briefly, 20μg of RNA was loaded onto 1.2% formaldehyde agarose gels and separated by gel electrophoresis. RNA was transferred to a Hybond-N+ membrane and crosslinked in a UV Stratalinker. The blot was prehybridized in Church mix at 55°C for 1 hour, followed by overnight hybridization with a Sty11 probe (de Lange, 1992). The blot was washed 3 times for 15 minutes at 55°C with Church wash and then exposed to a Phosphorimager screen for 5 days. Screens were scanned using ImageQuant software and quantified in Image J using the ethidium bromide stained 18S RNA as a loading control for normalization.

Microarray and qRT-PCR Analyses

Total RNA was isolated from cell lines using RNeasy Mini spin columns (QIAGEN) with DNase digestion, according to the manufacturer's instructions. Microarray hybridization and scanning were performed at the Genomics core facility at Rockefeller University, using Whole Human Genome DNA microarrays (Illumina HumanHT-12 v4). The data was analyzed using GeneSpring v12.6. Normalization was performed using quantiles and data was filtered to remove absent genes using flag calls. Experiments for HT1080 and HCT116 cell lines were performed in replicate, using two independent isolations of RNA. Differentially expressed genes were identified after performing moderated T-Tests and applying the Benjamini-Hochberg False Discovery Rate method. A further fold change of 3 or 2.75 was applied to the HT1080 and HCT116 clones respectively to identify genes that were highly transcriptionally deregulated due to the absence of Rap1. Microarrays for ARPE-19 were not performed in replicate and therefore an extremely stringent fold change threshold was applied to remove false negatives and identify differentially expressed genes, which were subsequently validated by qRT-PCR. For qRT-PCR, cDNA was prepared from 1μg of total RNA by using Thermoscript Reverse Transcriptase (Invitrogen). Quantitative PCR reactions were performed using Life Technologies SYBR Green Master Mix on an Applied Biosystems 7900HT Sequence Detection System. Differences between samples calculated using QuantStudio software (Applied Biosystems) using the ΔCT method and were normalized to GAPDH. Two independent isolations of RNA and reverse transcriptase reactions were conducted and the experiment was repeated six times for clones 23, 25, 30 and the parental cell line. The experiment for clone 26 was conducted in triplicate. Data was pooled to derive the mean averages and standard deviations. Significance was calculated using a two-tailed unpaired T-Test.

Supplemental References

Azzalin, C. M., Reichenbach, P., Khoriauli, L., Giulotto, E., and Lingner, J. (2007). Telomeric repeat containing RNA and RNA surveillance factors at mammalian chromosome ends. Science *318*, 798-801.

Celli, G. B., Lazzerini Denchi, E., and de Lange, T. (2006). Ku70 stimulates fusion of dysfunctional telomeres yet protects chromosome ends from homologous recombination. Nat Cell Biol *8*, 885-890.

de Lange, T. (1992). Human telomeres are attached to the nuclear matrix. Embo J *11*, 717-724.

de Lange, T., Shiue, L., Myers, R. M., Cox, D. R., Naylor, S. L., Killery, A. M., and Varmus, H. E. (1990). Structure and variability of human chromosome ends. Mol Cell Biol *10*, 518-527.

Dimitrova, N., and de Lange, T. (2006). MDC1 accelerates nonhomologous end-joining of dysfunctional telomeres. Genes Dev *20*, 3238-3243.

Karlseder, J., Smogorzewska, A., and de Lange, T. (2002). Senescence induced by altered telomere state, not telomere loss. Science *295*, 2446-2449.

Loayza, D., and de Lange, T. (2003). POT1 as a terminal transducer of TRF1 telomere length control. Nature *424*, 1013-1018.

Takai, K. K., Hooper, S., Blackwood, S., Gandhi, R., and de Lange, T. (2010). In vivo stoichiometry of shelterin components. J Biol Chem *285*, 1457-1467.

van Steensel, B., Smogorzewska, A., and de Lange, T. (1998). TRF2 protects human telomeres from end-to-end fusions. Cell *92*, 401-413.

Yang, D., Xiong, Y., Kim, H., He, Q., Li, Y., Chen, R., and Songyang, Z. (2011). Human telomeric proteins occupy selective interstitial sites. Cell Res *21*, 1013-1027.